

Sea level interannual variability along the west coast of India

I. Suresh¹, J. Vialard², M. Lengaigne^{2,3}, T. Izumo^{2,3}, V. Parvathi¹, and P.M. Muraleedharan¹

¹ CSIR-National Institute of Oceanography (CSIR-NIO), Goa, India

² LOCEAN-IPSL, Sorbonne Université (UPMC, Univ Paris 06)-CNRS-IRD-MNHN, Paris, France

³ Indo-French Cell for Water Sciences, IISc-NIO-IITM-IRD Joint International Laboratory, CSIR-NIO, Goa, India

Corresponding author: I. Suresh ,Physical Oceanography Division

CSIR - National Institute of Oceanography (CSIR-NIO)

Dona Paula – 403004, Goa, India

Email: isuresh@nio.org, isuresh.nio@gmail.com

Abstract

Interannual sea-level anomalies (SLA), and the related thermocline variations, along the west coast of India (WCI) strongly impact the ecosystems, fisheries, and potentially the monsoon rainfall. Here we investigate the mechanisms driving the WCI interannual SLA using a linear continuously-stratified ocean model, which realistically simulates the leading northern Indian Ocean SLA mode associated with the Indian Ocean Dipole (IOD). During, *e.g.*, positive IOD events, easterly wind anomalies near Sri Lanka in late summer and fall force downwelling coastal Kelvin waves, which induce positive WCI SLA within days. Meanwhile, equatorial easterlies force upwelling Kelvin waves that travel to WCI through Bay of Bengal coastal waveguide. Part of this opposite signal also transits slowly through Bay of Bengal interior as Rossby waves, eventually yielding negative SLA along the WCI in winter. The WCI SLA thus shifts from positive in fall to negative in winter during positive IOD events.

Plain language summary

The Indian Ocean Dipole (IOD) is the leading mode of Indian Ocean climate variability and is associated with anomalous winds over the equatorial Indian Ocean. A recent work has demonstrated that IOD events could strengthen or inhibit the upwelling of poorly oxygenated waters along the west coast of India (WCI). Such an upwelling impacts oxygen distribution in the upper layers and can thus have adverse effects on ecosystem and fisheries. Here we explain the mechanisms linking the IOD to upwelling along the WCI. IOD zonal winds in the central equatorial Indian Ocean produce two opposite signals on WCI. One that travels fast, directly up the WCI during summer and fall. But another opposite-polarity signal follows equator and Bay of Bengal rim - a part of which transits slowly through the Bay of Bengal interior, eventually reaching the WCI and flipping the sign of sea-level anomalies there in winter.

Key Points: Positive Indian ocean dipoles induce positive (negative) sea level anomalies in boreal fall (winter) along the west coast of India.

- Fall easterly wind anomalies near Sri Lanka force *downwelling* coastal Kelvin waves that travel quickly to the west coast of India
- Fall eastern equatorial *upwelling* signals travel more slowly through the interior Bay of Bengal, reaching the Indian west coast in winter

Keywords: West coast of India, Sea level, Interannual variability, Indian Ocean Dipole, coastal waveguide, local and remote forcing.

Accepted in *Geophysical Research Letters* on 13 November 2018

1. Introduction

The West Coast of India (WCI) experiences a seasonal, coastal upwelling, peaking in boreal fall (Schott & McCreary, 2001). Enhanced productivity during this period strongly supports regional fisheries (Banse, 1959), making it important from a socio-economical viewpoint. This has motivated research on the mechanisms responsible for this seasonal upwelling. Early observational studies (Sharma, 1968; Banse, 1968) noticed a mismatch between upwelling and local winds, suggesting a strong influence of remote forcing. Modeling studies later highlighted significant remote contributions from seasonal winds in Bay of Bengal (BoB/Bay), with signals from BoB propagating around southern tip of India to the WCI as coastal Kelvin waves (McCreary et al., 1993; Shankar et al., 2002). Suresh et al. (2016) further demonstrated that seasonal wind variations in a small region near southern tip of India and Sri Lanka (STIP region) drive a large fraction (60%) of the WCI sea level seasonal cycle, and hence of the upwelling intensity since the sea-level variability is a good proxy of thermocline depth variations (Shankar, 2000).

The WCI interannual sea-level variability has received considerably less attention than seasonal variability, partly because of its relatively weaker amplitude (Fig. S1). Parvathi et al. (2017) however demonstrated that this weak WCI variability, when it combines with the shallowest thermocline in fall (peak upwelling), can have strong socio-economic impacts. Beyond modulating intensity of seasonal upwelling and the associated productivity, WCI fall interannual sea-level anomalies (SLA) modulate occurrence of coastal anoxic (complete depletion of oxygen) events (Parvathi et al., 2017), which have tremendous consequences on fisheries and ecosystems (Naqvi et al., 2000; 2009). The Arabian Sea indeed hosts one of the three major open-ocean Oxygen Minimum Zones globally, resulting from high oxygen consumption associated with remineralization of sinking organic matter in this highly productive region, and relatively poor ventilation of subsurface layers (Resplandy et al., 2012). The seasonal upwelling brings these hypoxic waters to the wide WCI continental shelf to form the largest natural coastal hypoxic system in the world ocean during fall (Naqvi et al., 2000). The hypoxic conditions become more severe during some years, leading to coastal anoxia, with deleterious impacts on ecosystem and fisheries (Naqvi et al., 2009).

In addition to these strong biological impacts, interannual SLA along the WCI may also have important consequences for the regional climate. The WCI SLAs propagate westward as Rossby waves into the southeastern Arabian Sea (Shankar & Shetye, 1997; Suresh et al., 2016), where they induce thermocline-depth perturbations, hence potentially influencing local sea surface temperature and thus monsoon rainfall. For instance, the southeastern Arabian Sea is home to a *mini warm pool* in spring that influences both Indian summer monsoon onset date and rainfall (Durand et al., 2004;

Masson et al., 2005; Vinayachandran et al., 2007), thereby impacting livelihood of more than one billion inhabitants of the Indian subcontinent.

These strong socio-economic impacts call for a thorough analysis of interannual sea-level variations along the WCI. However, most past studies focused on the BoB (Aparna et al., 2012), where the SLA interannual variability is stronger than that along the WCI (Fig. S1b). Clarke & Liu (1994) were the first to suggest that remote equatorial wind forcing could induce coherent interannual SLAs along the 8000-km stretch of the northern Indian Ocean coast. Equatorial zonal wind variations indeed drive equatorial Kelvin waves. Upon reflecting into Rossby waves at the Sumatra coast, part of the impinging wave energy propagates around BoB rim as coastal Kelvin waves and into the BoB interior as Rossby waves, a pathway similar to that at seasonal timescale (Shankar et al., 2002). Han & Webster (2002) further demonstrated that remote equatorial forcing dominates interannual SLA in the eastern BoB, while local and remote equatorial forcing contribute equally in the western BoB.

Aparna et al. (2012) further pointed out that the BoB interannual SLA variations largely co-occur with the two main interannual climate modes affecting the Indian Ocean (Schott et al., 2009): the Indian Ocean Dipole (IOD; Saji et al., 1999; Webster et al., 1999) and the El Niño - Southern Oscillation (ENSO), which influences the Indian Ocean through atmospheric teleconnection (Klein et al., 1999). A positive IOD induces negative SLA in the BoB during April-December, with a peak in fall (Aparna et al., 2012). Due to the tendency of ENSO to trigger IOD (Annamalai et al., 2003), it is difficult to clearly attribute these sea-level variations to either ENSO or IOD influence. Several studies used partial correlation techniques to isolate intrinsic SLA signals associated with ENSO and IOD (Yu et al., 2005; Rao & Behera, 2005; Currie et al., 2013). They found that ENSO-induced wind variations are weaker and further south relative to those associated with IOD, so that the IOD dominates oceanic interannual variability in the northern Indian Ocean.

Parvathi et al. (2017) is to our knowledge the only study that investigated the WCI interannual thermocline (hence SLA) variability, owing to its strong impact on anoxic events there. They found that the fall IOD-induced easterly wind anomalies near southern tip of India were well correlated with WCI interannual SLA, favoring downwelling anomalies (during positive IOD). They proposed a mechanism, similar to that at seasonal timescale (Suresh et al., 2016), in which the zonal wind-stress variations at southern tip of India force coastal Kelvin waves that travel to the WCI. They have however neither demonstrated it, nor worked out the relative contributions from local winds and remote forcing from STIP, BoB or equatorial regions. Given their strong societal implications, interannual sea-level variations along the WCI need to be thoroughly described and understood. This

is the goal of this paper. Section 2 describes our linear ocean model and related sensitivity experiments that allow us to isolate the aforementioned processes. Section 3 describes the IOD influence on the WCI interannual SLA variability and identifies its main remote and local forcing mechanisms. Section 4 summarizes and discusses our main findings.

2. The model and methods

We use a modified version of the linear, continuously-stratified ocean model of McCreary et al. (1996), which we previously used for studying the northern Indian Ocean intraseasonal sea-level variability (Suresh et al., 2013) and sea level seasonal cycle along the WCI (Suresh et al., 2016). Shallow water equations are solved for the first five baroclinic modes at 0.25° -resolution over the Indian Ocean (30°S – 30°N , 30°E – 110°E), with a coastline derived from 200-m isobaths. The model solution is obtained as the sum of these modes (summing first 20 modes gives similar results, not shown). The model is forced with daily TropFlux wind-stress (Praveen Kumar et al., 2013) anomalies relative to long-term mean over 1979-2013. This solution is referred to as the control (CTL) experiment. The model reproduces very well the basin-scale sea-level variability in the northern Indian Ocean at intraseasonal (Suresh et al., 2013) and seasonal (Suresh et al., 2016) timescales. Its performance at interannual timescale will be assessed in Section 3.1.

Arabian Sea (local) wind forcing and remote forcing from the equatorial, BoB, and STIP regions can all influence the WCI SLA variability. Each of those contributions can further be decomposed into that resulting from alongshore forcing at the coast and that from wind-stress curl in the interior ocean. The sensitivity experiments and decomposition method used to separate these processes are the same as in Suresh et al. (2016), and are further described in the supporting information. The pathways of each of those signals, and the associated forcing hotspots, will be detailed in Section 3.2. Our results are not very sensitive to other reasonable choices of model parameters or dampers used in sensitivity experiments (not shown).

Interannual signals are obtained by applying a band-pass filtering with cutoff period of 150-day to 7-year, after subtracting mean seasonal cycle and detrending 1979-2013 time series. The interannual CTL SLA is validated against AVISO merged multi-satellite delayed mode product. These observations include effects of meso-scale eddies in, e.g., western BoB or Arabian Sea (Chelton et al. 2011), unlike our linear model. We isolate large-scale interannual SLA signals in the Indian Ocean north of 20°S using empirical orthogonal function (EOF) analysis. In order to relate this signal to climate variability associated with IOD or ENSO, we respectively use Dipole Mode Index (DMI) averaged over September-November (SON; the peak season of IOD) and Multivariate

ENSO Index (MEI) averaged over November-January (NDJ; the peak season of ENSO), normalized by their respective standard deviations.

3. Origin and processes of WCI interannual sea-level variability

3.1 The IOD influence

Figure 1 displays the first EOF (EOF1) spatial pattern and principal component (PC1) from CTL and observations. The EOF1 is well separated from higher-order modes in both model and observations: it indeed explains 64% (53%) of total SLA variance in CTL (observations), while second mode explains only 10% (9%). The overestimated percentage of explained variance in model compared to that in observations results from linearity of the model that does not simulate meso-scale eddies, while observed SLA contains many eddies throughout the basin (Chelton et al., 2011). Apart from that, there is a remarkable agreement between modeled and observed leading EOF patterns (Fig. 1ab, pattern correlation of 0.89). Figure 1ab also displays the wind stresses associated with this leading mode of interannual SLA (obtained through linear regression of interannual wind-stress anomalies onto PC1). The model and observations both indicate that the leading mode of interannual SLA in the Indian Ocean is associated with equatorial zonal wind-stress anomalies. We will hereon describe results for the above patterns of SLA and winds, although our analysis is equally valid for opposite SLA and wind polarities. These easterly wind-stress anomalies induce upwelling Kelvin wave response in the eastern equatorial Indian Ocean, with one part of the signal propagating into northern Indian Ocean coastal waveguide as coastal Kelvin wave that can be tracked all the way to the Sri Lankan coast (Fig. 1ab). The equatorial easterly anomalies also induce downwelling equatorial Rossby wave response to the west. Due to asymmetric wind forcing around the equator (10°S - 6°N), the SLA response is more pronounced in the southern hemisphere. The model underestimates this positive SLA response, but compares reasonably well with observations in the northern hemisphere, including the WCI. Finally, temporal variations associated with this leading mode are strikingly similar between modeled and observed PC1, with a 0.97 correlation (Fig. 1c).

The leading SLA mode and associated wind signals (Fig. 1ab) are reminiscent of those associated with a positive IOD (Webster et al., 1999; Murtugudde et al., 2000). As noted in introduction, there is a tendency for ENSO to trigger IOD (Annamalai et al., 2003), making it difficult to isolate intrinsic SLA signals associated with IOD (i.e. IOD occurring without ENSO forcing) from those associated with ENSO (i.e. driven by ENSO teleconnections, when they fail to trigger IOD). Previous studies (Yu et al., 2005; Rao & Behera 2005; Currie et al., 2013) have however demonstrated that most of the northern Indian Ocean interannual SLA and thermocline

variations are mainly driven by IOD-related wind signals. In line with those studies, both observed and modeled SON PC1 exhibit higher correlation with SON DMI (~ 0.95) than with NDJ MEI (0.81; Fig. S2), corroborating that EOF1 is associated with IOD intrinsic variability, rather than ENSO.

The typical temporal evolution of IOD-related SLA patterns can be obtained through a lead/lag regression onto SON DMI. We will focus on describing those typical signals in October (Fig. 2a; during IOD peak, also representative of IOD growth in summer) and in February (Fig. 2f; after IOD termination) as these two periods display opposite SLA along the WCI. Positive IODs are associated with positive SLAs along the WCI in October (Fig. 2a) and negative SLAs in February (Fig. 2f). The October SLA pattern is very similar to that on Figure 1a described above. By February, IOD-induced equatorial easterly wind anomalies have largely disappeared. Negative SLA signals persist over the entire eastern Indian Ocean, including in the BoB and along the WCI. In the next subsection, we will use dedicated model sensitivity experiments to understand the dynamics involved in this evolution, with a specific focus on the WCI, where SLAs have strong societal impacts.

3.2 Processes of IOD-induced interannual sea-level variations

We isolate contributions from various forcing regions to interannual SLA anomalies in the northern Indian Ocean, or specifically along WCI, following the same strategy as in Suresh et al. (2016) (more details in supporting information). The pathways linking each forcing region to WCI are shown schematically on Figure 2. We will briefly remind those pathways. Equatorial zonal winds trigger Kelvin waves that travel to the eastern boundary, where a part of the energy gets reflected back as equatorial Rossby waves (dashed light-blue arrows at lowest latitude on Fig. 2c) and another part propagates into the BoB as coastal Kelvin waves. Part of this BoB signal follows the BoB rim and further propagates around Sri Lanka to the WCI as coastal Kelvin waves (continuous light-blue arrow on Fig. 2c). A fraction of coastal Kelvin-wave energy on the eastern BoB rim is radiated westward as Rossby waves (dashed light-blue arrows on Fig. 2c). This signal takes considerably longer time to reach the Indian east coast than Kelvin-wave signal that follows the coastal waveguide. For example, a long non-dispersive first mode baroclinic Rossby wave would take ~ 60 (~ 100) days to cross the BoB at 8°N (10°N ; Fig. S4), while a first baroclinic mode coastal Kelvin wave (with a typical speed of 2.5 m.s^{-1}) would take less than 20 days to travel the ~ 4000 -km distance separating the Andaman Sea from Sri Lanka along the shelf break. These coastal Kelvin waves then take less than a week to travel from Sri Lanka to the WCI northern end. These signals associated with remote equatorial forcing will be referred to as EQ.

BoB wind variations force signals that include coastal Kelvin waves resulting from alongshore

wind variations (ABB; continuous green line on Fig. 2d) and Rossby waves induced by Ekman pumping in the BoB interior (IBB; dashed green line on Fig. 2d) (McCreary et al., 1996; Suresh et al., 2016). The above signals associated with BoB forcing will be named BB.

As demonstrated by Suresh et al. (2016) for the seasonal timescale, STIP wind variations can also induce coastal Kelvin waves, either directly through alongshore forcing (AST; continuous purple line on Fig. 2b) or indirectly through Rossby waves forced by strong wind-stress curl east of Sri Lanka (IST; dashed purple line on Fig. 2b). We will name this process ST. We will also isolate the effect of Arabian Sea wind forcing (AS), which reduces to local alongshore forcing for WCI (wind-stress curl forces Rossby waves further west in the interior Arabian Sea).

We will now examine how the aforementioned processes contribute to the IOD-induced interannual SLA along the WCI (estimated as lead/lag regression of CTL interannual SLA onto SON-averaged DMI; regression onto SON-averaged PC1 gives similar results). Figure 2 presents maps of these process contributions for October and February, while Figure 3 displays time-series of those contributions to WCI SLA during a typical positive IOD. ST and EQ are the dominant processes driving the IOD-related WCI interannual SLA (plus a weaker AS contribution almost in phase with ST, non-negligible in late summer and early fall; Fig. 3a). During a positive IOD, the WCI SLA sign changes from positive during late summer and fall to negative during winter both in CTL and observations (Fig. 3a). ST induces positive SLA along the WCI, with its contribution peaking in October-November (Fig. 3a). In contrast, EQ induces negative SLA that peaks later in December-January (Fig. 3a). The tradeoff between positive ST and delayed negative EQ SLAs determines the WCI SLA change of sign from boreal fall to winter.

During late summer and fall, equatorial easterly wind-stress anomalies during a positive IOD extend off the equator to $\sim 10^\circ\text{N}$ (Fig. 2a), leading to strong alongshore forcing in the STIP region (Fig. S3cd). The resulting northward Ekman transport towards the coast induces downwelling coastal Kelvin waves (i.e. AST). Meanwhile, the poleward decrease of easterly wind anomalies leads to strong negative wind-stress curl (Figs. 2a, S3d) east of Sri Lanka, inducing downwelling Rossby waves that reach the Sri Lankan coast within 1-2 weeks and trigger downwelling coastal Kelvin waves (i.e. IST). The resulting downwelling ST signals (Fig. 2b) propagate northward along the WCI as coastal Kelvin waves. AST and IST signals are in phase and both contribute nearly equally to ST (Fig. 3b). While the peak of ST forcing (Fig. S3cd) coincides with the typical IOD peak in October, its contribution along the WCI peaks in November (Fig. 3), as the ocean is an integrator of wind forcing. The ST contribution to WCI starts decreasing in December (Fig. 3), coinciding with the IOD termination and disappearance of STIP wind anomalies (Fig. S3ef).

EQ is due to equatorial easterlies during a positive IOD, inducing upwelling in the eastern equatorial Indian Ocean, with part of this signal propagating into the BoB coastal waveguide as coastal Kelvin waves (Fig. 2c). Coastal Kelvin wave takes ~25 days to travel the ~5500-km of coastal waveguide between the eastern Indian Ocean and the WCI (at 10°N), with the typical speed (2.5 m.s^{-1}) of first baroclinic mode. Part of the upwelling EQ signal thus reaches the WCI within a month and interferes destructively with downwelling ST signal (Figs. 2bc and 3a), thereby decreasing CTL SLA during November. Meanwhile, part of the EQ negative SLA on the BoB eastern rim radiates westward into interior Bay as upwelling Rossby waves (Fig. 2c). As noted earlier, Rossby waves take ~2 months at 8°N to ~6 months northward of 14°N to cross the Bay (Fig. S4). This explains why the EQ contribution to WCI peaks in December-February (roughly 2-3 months after the peak of IOD equatorial wind anomalies) and dominates the CTL SLA after ST has receded. EQ continues to contribute to CTL SLA until March-April when equatorial wind anomalies have completely receded (Figs. 2f and S3g). The slow propagation of this fraction of the EQ signal through interior BoB as Rossby waves thus explains the delayed EQ contribution to CTL negative SLA along the WCI during winter and the following spring.

The AS and BB processes contribute only weakly to WCI SLA. AS is due to the relatively weak IOD-induced WCI alongshore forcing (Fig. 2a; poleward weakening of WCI winds upto 15°N, yielding weak positive SLA on Figs. 2e and 3a; non-negligible only during late summer and fall). The BB contribution is even weaker due to opposing contributions from alongshore (ABB) and interior (IBB) BoB forcing (Fig. 3b). The anomalous anticyclonic wind circulation in BoB (Fig. 2a) indeed yields negative wind-stress curl (Fig. S3d) that forces downwelling IBB signals in the southern BoB (Fig. 2d). The above anticyclonic circulation (Fig. 2a) is also associated with upwelling-favorable alongshore winds all around the BoB rim, especially along the northwestern boundary (Fig. S3d), yielding negative ABB signals (Fig. 2d). These two opposite signals result in overall weak BB remote forcing contribution to WCI SLA during fall and winter (Fig. 3b).

4. Summary and discussion

Parvathi et al. (2017) recently demonstrated that IOD events could modulate the thermocline (and oxycline) depth anomalies along the WCI during fall and thus favor or inhibit anoxia along the WCI. It is therefore important to understand the processes by which IOD influences the WCI. Parvathi et al. (2017) hypothesized a key role of zonal wind variations near the southern tip of India, as that previously demonstrated for the seasonal cycle (Suresh et al., 2016), but did not demonstrate it. Here, we use a linear ocean model to explore the main processes that influence interannual SLA (and hence thermocline/oxycline variations) along the WCI during an IOD event. The leading mode

of interannual SLA variability in the Indian Ocean is associated with the IOD and is very well reproduced by our model. A typical positive IOD is associated with positive SLAs off the WCI in late summer and fall, and negative anomalies in following winter and spring. Equatorial easterly wind anomalies typical of positive IODs extend sufficiently northward to STIP region to trigger downwelling coastal Kelvin waves, which dominate WCI SLA during late summer and fall. Part of the upwelling Kelvin waves driven by equatorial easterlies propagates into BoB, and then transits slowly (2-6 months) as westward Rossby waves through BoB interior. At the western BoB rim, those Rossby waves excite upwelling coastal Kelvin waves, which bend around Sri Lanka and propagate to WCI. This delayed negative signal, which has so far not been discussed in the literature, dominates the WCI SLA during the winter and spring following positive IOD events.

Aparna et al. (2012) had remarked that negative IODs were associated with smaller SLAs than their positive counterpart in BoB. Along the same lines, Parvathi et al. (2017) reported an asymmetric influence of positive and negative IOD events on WCI oxycline/thermocline variations, with positive IODs suppressing anoxia while negative IODs having a less systematic impact. They attributed this asymmetry to weaker wind anomalies near southern tip of India during negative IODs, in relation with the skewed nature of IOD itself (Saji & Yamagata, 2003). Our model allows us to further investigate the processes responsible for this asymmetry (Fig. S5). The ST contribution is indeed weaker for negative than for positive IODs, as hypothesized by Parvathi et al. (2017), but only by ~20%, while the total SLA is weaker by ~60%. Our decomposition further shows that BB contribution is almost negligible or negative for negative IOD, also explaining a large part of the asymmetry. On the other hand, the EQ contribution remains nearly symmetric, suggesting that equatorial zonal wind-stress anomalies have roughly similar magnitudes for positive and negative IODs, but they extend further north towards STIP and BoB during positive IODs.

Previous studies that investigated the mechanisms of interannual SLA variations in the northern Indian Ocean (Aparna et al., 2012; Clarke & Liu, 1994; Han & Webster, 2002) focused on BoB. Though our study focuses on WCI, we discuss the results for BoB (Figs. 2 and S6ab) for consistency with those studies. All those studies emphasized the importance of remote equatorial forcing for BoB interannual SLA. Han & Webster (2002) showed that equatorial forcing dominates the SLA variability along BoB eastern rim. We find that eastern BoB CTL SLA is entirely due to EQ (Fig. S6a). They further found a growing influence of BoB forcing counterclockwise around the Bay, as we do. At the east coast of India, for instance, SLA interannual variability is still dominated by EQ, but with a non-negligible contribution from BB (Fig. S6b). This good agreement between our study and the previous ones for BoB further strengthens confidence in our results for the WCI.

As noted in introduction, SST variations in southeastern Arabian Sea could influence rainfall over India. It is hence worth examining the mechanisms contributing to SLA variability in this region, as those SLAs can influence SST through thermocline feedback and advection associated with passing planetary waves. Southeastern Arabian Sea is downstream along the path of Rossby waves radiated at low latitudes from the WCI (Shankar & Shetye, 1997; Suresh et al., 2016) and hence the SLA evolution during IOD and the underlying processes (Fig. S6c) are very similar to those along the WCI (Fig. 3a), with slightly higher contribution from interior Arabian Sea forcing (Figs. 2ej and S6c) as could be expected. A positive IOD thus induces positive SLA in late summer and fall and negative SLA during the following winter and spring in southeastern Arabian Sea. This modeling result is in line with the XBT observations of strong negative subsurface temperature anomalies in this region from December 2006 to summer 2007 (Gopalakrishna et al., 2010), in both timing and sign, following the strong positive IOD in fall 2006. Besides its potential instantaneous impact on late summer rainfall, the delayed IOD influence could also potentially modulate subsurface conditions in the *Arabian Sea mini-warm pool* (Vinayachandran et al., 2007) in the following spring, which could in turn feedback onto Indian summer monsoon characteristics. This would be further investigated in a future study.

Acknowledgements

Authors thank Director, CSIR-NIO. IS thanks Neetu and Sadhvi, and acknowledges financial support from ESSO-INCOIS/MoES (HOOFS), NRB/DRDO and CSIR, New Delhi. JV, ML and TI acknowledge financial support from Institut de Recherche pour le Développement (IRD) and CNES-Altika project. This work was done while ML and TI were visiting scientists at CSIR-NIO supported by IRD funding. JV acknowledges IRD for supporting regular visits to CSIR-NIO and CSIR-NIO for *Adjunct Scientist*. VP acknowledges CSIR senior research fellowship. Authors thank the reviewers for their constructive comments. A more detailed discussion can be found in the supporting information (Locarnini et al., 2010; Smith & Sandwell, 1997). The manuscript uses Tropflux wind stresses from www.incois.gov.in/tropflux/, sea-level observations from www.aviso.oceanobs.com/fr/accueil/index.html, Dipole Mode Index from www.jamstec.go.jp/frcgc/research/d1/iod/DATA/dmi.monthly.txt and Multivariate ENSO Index from www.esrl.noaa.gov/psd/enso/mei/table.html. This is NIO contribution #####.

Figure 1. Leading EOF of interannual SLAs in the Indian Ocean from a) model CTL experiment and b) satellite-altimeter observations; c) associated normalized PC1 (model-black, observations-red). The associated wind-stress anomalies on panels a and b are obtained through regression of interannual wind stresses onto normalized PC1. The black box, which is representative of the WCI and used in Figure 3, is marked on panel a.

Figure 2. Typical IOD basin-scale SLAs and contributions from forcing in various regions, obtained as lead/lag regressions of the (a-e) October and (f-j) February interannual anomalies onto normalized SON-averaged DMI for (a,f) CTL SLA and windstresses and decomposition of CTL SLA into (b,g) STIP forcing or ST process (purple box and arrows); (c,h) equatorial forcing or EQ process (light blue); (d, i) BoB forcing or BB process (green); and (e,j) Arabian Sea forcing or AS process (red). The ST, EQ, BB and AS contributions add up to CTL, owing to model linearity. Arrows symbolize the pathways of equatorial and coastal Kelvin waves (continuous) and Rossby waves (dashed).

Figure 3. Typical IOD SLA along WCI and contributing processes, obtained as lead/lag regressions of interannual SLA (*cm*) on WCI box (Fig. 1a) to normalized SON-averaged DMI for (a) CTL (continuous black), with its observed counterpart (dashed black), and its decomposition into ST (purple), EQ (light blue), BB (green), and AS (red) processes. (b) BB and AS processes (thick continuous) are further decomposed into alongshore (thin continuous) and interior wind-stress curl (thin dashed) forcing contributions. The grey vertical strips mark October and February, for which basin-scale patterns are displayed on Figure 2.

References

- Annamalai, H., Murtugudde, R., Potemra, J., Xie, S. P., Liu, P., & Wang, B. (2003). Coupled dynamics over the Indian Ocean: spring initiation of the Zonal Mode. *Deep-Sea Res. Pt. II*, *50*, 2305–2330, doi:10.1016/S0967-0645(03)00058-4.
- Aparna, S. G., McCreary, J. P., Shankar, D., & Vinayachandran, P. N. (2012). Signatures of Indian Ocean Dipole and El Niño–Southern Oscillation events in sea level variations in the Bay of Bengal, *J. Geophys. Res.*, *117*, C10012, doi:10.1029/2012JC008055.
- Banse, K. (1959). On upwelling and bottom-trawling off the south west coast of India. *J. Mar. Biol. Assoc. India*, *1*, 33–49.
- Banse, K. (1968). Hydrography of the Arabian Sea shelf of India and Pakistan and effects on demersal fishes. *Deep Sea Res. Oce-anogr. Abstr.*, *15*, 45–79.
- Chelton B. D., Schlax, M. G., & Samelson, R. M. (2011). Global observations of nonlinear mesoscale eddies. *Progress in Oceanography*, *91*, 167-216.
- Clarke, A. J., & Liu, X. (1994). Interannual sea level in the northern and eastern Indian Ocean. *J. Phys. Oceanogr.*, *24*, 1224–1235.
- Currie, J. C., Lengaigne, M., Vialard, J., Kaplan, D. M., Aumont, O., Naqvi, S. W. A., & Maury, O. (2013). Indian Ocean Dipole and El Niño/Southern Oscillation impacts on regional chlorophyll anomalies in the Indian Ocean. *Biogeosciences*, *10*, 6677–6698, doi:10.5194/bg-10-6677-2013.
- Durand, F., Shetye, S. R., Vialard, J., Shankar, D., Shenoi, S. S. C., Ethe, C., & Madec, G. (2004). Impact of temperature inversions on SST evolution in the South-Eastern Arabian Sea during pre-summer monsoon season. *Geophys. Res. Lett.*, *31*, doi:10.1029/2003GL018906.
- Gopalakrishna, V.V., Durand, F., Nisha, K., Lengaigne, M., Boyer, T. P., Costa, J., Rao, R.R., Ravichandran, M., Amrithash, S., John, L., Girish, K., Ravichandran, C., & Suneel, V. (2010). Observed intra-seasonal to interannual variability of the upper ocean thermal structure in the southeastern Arabian Sea during 2002-2008. *Deep-Sea Res. I*, *57*, 739-754.
- Han, W., & Webster, P. J. (2002). Forcing mechanisms of sea level interannual variability in the Bay of Bengal. *J. Phys. Oceanogr.*, *32*, 216–239.
- Klein, S. A., Soden, B. J., & Lau, N.-C. (1999). Remote sea surface temperature variations during ENSO: Evidence for a tropical atmospheric bridge. *J. Climate*, *12*, 917–932.
- Locarnini, R. A., Mishonov, A. V., Antonov, J. I., & Boyer, T. P. (2010). World Ocean Atlas 2009, Volume 1: Temperature. Levitus, S., Ed. NOAA Atlas NESDIS 68, U.S. Government Printing Office, Washington, D.C., 184 pp.
- Masson, S., Luo, J.-J., Madec, G., Vialard, J., Durand, F., Gualdi, S., Guilyardi, E., Behera, S., Delecluse, P., Navarra, A., & Yamagata, T. (2005). Impact of barrier layer on winter-spring variability of the southeastern Arabian Sea. *Geophys. Res. Lett.*, *32*, L07703, doi:10.1029/2004GL021980.
- McCreary, J. P., Han, W., Shankar, D., & Shetye, S.R. (1996). Dynamics of the East India Coastal

- Current. 2. Numerical solutions. *J. Geophys. Res.*, *101*, 13,993–14,010, doi:10.1029/96JC00560.
- McCreary, J. P., Jr., Kundu, P.K., & Molinari R.L. (1993). A numerical investigation of dynamics, thermodynamics and mixed-layer processes in the Indian Ocean, *Prog. Oceanogr.*, *31*(3), 181–244, doi:10.1016/0079-6611(93)90002-U.
- Naqvi, S. W. A., Jayakumar, D. A., Narvekar, P. V., Naik, H., Sarma, V. V. S. S., D’Souza, W., Joseph, S., & George, M. D. (2000). Increased marine production of N₂O due to intensifying anoxia on the Indian continental shelf. *Nature*, *408*, 346–349.
- Naqvi, S. W. A., Naik, H., Jayakumar, D. A., Pratihary, A. K., Narvenkar, G., Kurian, S., Agnihotri, R., Shailaja, M. S., & Narvekar, P. V. (2009). Seasonal anoxia over the Western Indian continental shelf. *Geophysical Monograph Series*, *185*, 10.1029/2008GM000745.
- Parvathi, V., Suresh, I., Lengaigne, M., Ethe, C., Vialard, J., Levy, M., Neetu, S., Aumont, O., Resplandy, L., Naik, H., & Naqvi, W. (2017). Positive Indian Ocean Dipole events prevent anoxia along the west coast of India. *Biogeosciences*, *14* (6), 1541-1559, <https://doi.org/10.5194/bg-14-1541-2017>.
- Praveen Kumar, B., Vialard, J., Lengaigne, M., Murty, V. S. N., McPhaden, M. J., Cronin, M., Pinsard, F., & Gopala Reddy, K. (2013). TropFlux wind stresses over the tropical oceans: evaluation and comparison with other products. *Clim. Dyn.*, *40*, 2049-2071.
- Rao, S. A., & Behera, S. K. (2005). Subsurface influence on SST in the tropical Indian Ocean: structure and inter-annual variability. *Dynam. Atmos. Oceans*, *39*, 103–135, doi:10.1016/j.dynatmoce.2004.10.014, 2005.
- Resplandy, L., Lévy, M., Bopp, L., Echevin, V., Pous, S., Sarma, V. V. S. S., & Kumar, D. (2012). Controlling factors of the oxygen balance in the Arabian Sea’s OMZ. *Biogeosciences*, *9*, 5095–5109, doi:10.5194/bg-9-5095-2012, 2012.
- Saji, N. H., Goswami, B. N., Vinayachandran, P. N., & Yamagata, T. (1999). A dipole mode in the tropical Indian Ocean. *Nature*, *401*, 360–363, 1999.
- Saji, N.H., & Yamagata, T. (2003). Structure of SST and surface wind variability during Indian Ocean Dipole Mode years: COADS observations. *J. Clim.*, *16*, 2735–2751.
- Schott, F.A., & McCreary, J. P. (2001). The monsoon circulation of the Indian Ocean. *Prog. Oceanogr.*, *51*, 1–123.
- Schott, F. A., Xie, S.-P., & McCreary, Jr. J. P. (2009). Indian Ocean circulation and climate variability. *Rev. Geophys.*, *47*, RG1002, doi:10.1029/2007RG000245.
- Shankar, D. (2000). Seasonal cycle of sea level and currents along the coast of India, *Current Science*, *78*(3), 279-288.
- Shankar, D., & Shetye, S.R. (1997). On the dynamics of the Lakshadweep high and low in the southeastern Arabian Sea. *J. Geophys. Res.*, *102*(C6), 12551, doi:10.1029/97JC00465.
- Shankar, D., Vinayachandran, P.N., & Unnikrishnan, A.N. (2002). The monsoon currents in the north Indian Ocean. *Prog. Oceanogr.*, *52*(1), 63–120, doi:10.1016/S0079-6611(02)00024-1.

- Sharma, G.S. (1968). Seasonal variation of some hydrographic properties of the shelf waters off the west coast of India. *Bull. Nat. Inst. Sci. India*, 38, 263–275.
- Smith, W.H. F., & Sandwell, D.T. (1997). Global sea floor topography from satellite altimetry and ship depth soundings. *Science*, 277, 5334.
- Suresh, I., Vialard, J., Izumo, T., Lengaigne, M., Han, W., McCreary, J., & Muraleedharan, P. M. (2016). Dominant role of winds near Sri Lanka in driving seasonal sea level variations along the west coast of India. *Geophys. Res. Lett.*, 43, doi:10.1002/2016GL069976.
- Suresh, I., Vialard, J., Lengaigne, M., Han, W., McCreary, J., Durand, F., & Muraleedharan P.M. (2013). Origins of wind-driven intraseasonal sea level variations in the North Indian Ocean coastal waveguide. *Geophys. Res. Lett.*, 40, 5740–5744, doi:10.1002/2013GL058312.
- Vinayachandran, P. N., Shankar, D., Kurian, J., Durand, F., & Shenoi, S. S. C. (2007). Arabian Sea mini warm pool and the monsoon onset vortex. *Curr. Sci.*, 93(2), 203–214.
- Webster, P. J., Moore, A. M., Loschnigg, J. P., & Leben, R.R. (1999). Coupled oceanic– atmospheric dynamics in the Indian Ocean during 1997– 98. *Nature*, 401, 356– 360.
- Yu, W., Xiang, B., Liu, L., & Liu, N. (2005). Understanding the origins of interannual thermocline variations in the tropical Indian Ocean. *Geophys. Res. Lett.*, 32, 24706, doi:10.1029/2005GL024327.

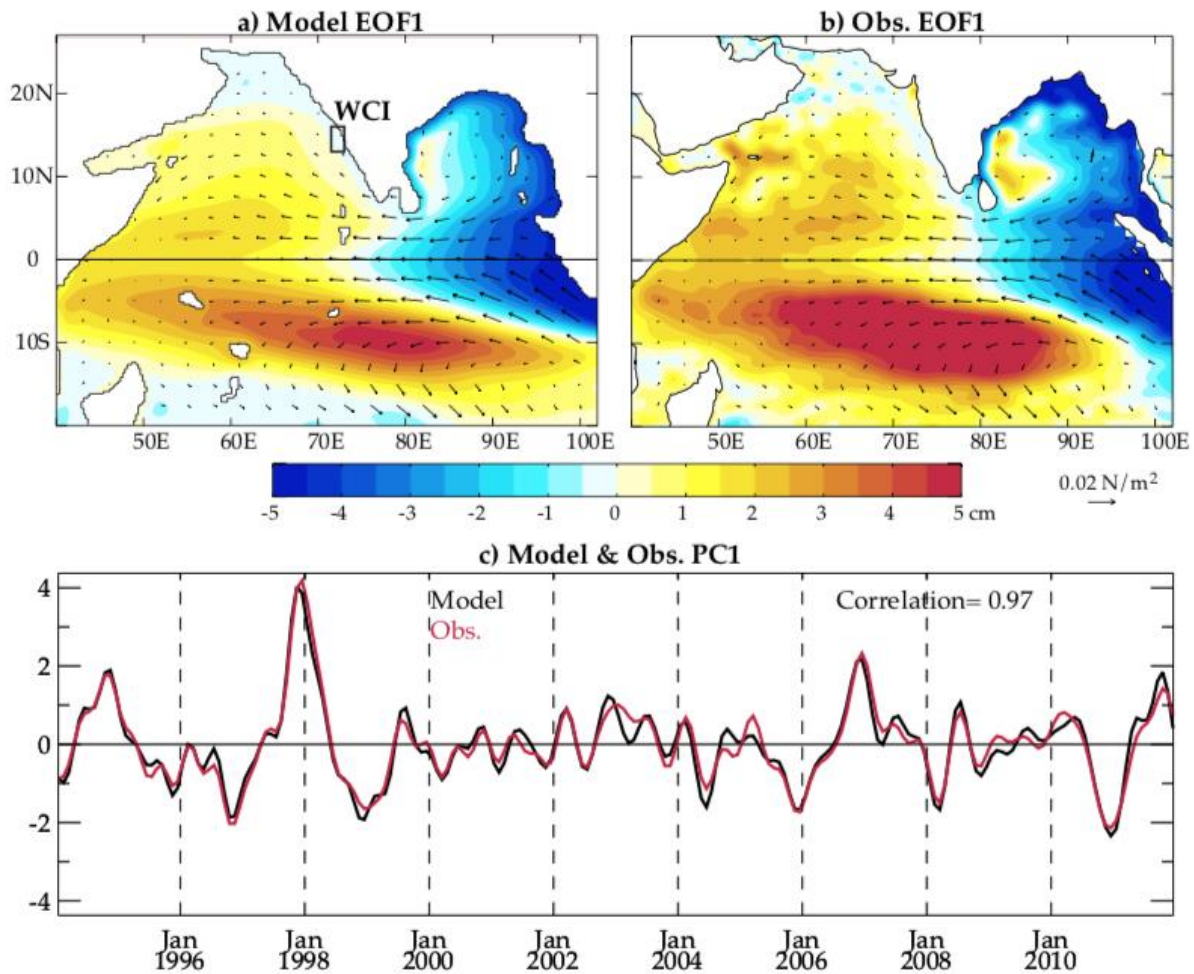


Figure 1. Leading EOF of interannual SLAs in the Indian Ocean from a) model CTL experiment and b) satellite-altimeter observations; c) associated normalized PC1 (model-black, observations-red). The associated wind-stress anomalies on panels a and b are obtained through regression of interannual wind stresses onto normalized PC1. The black box, which is representative of the WCI and used in Figure 3, is marked on panel a.

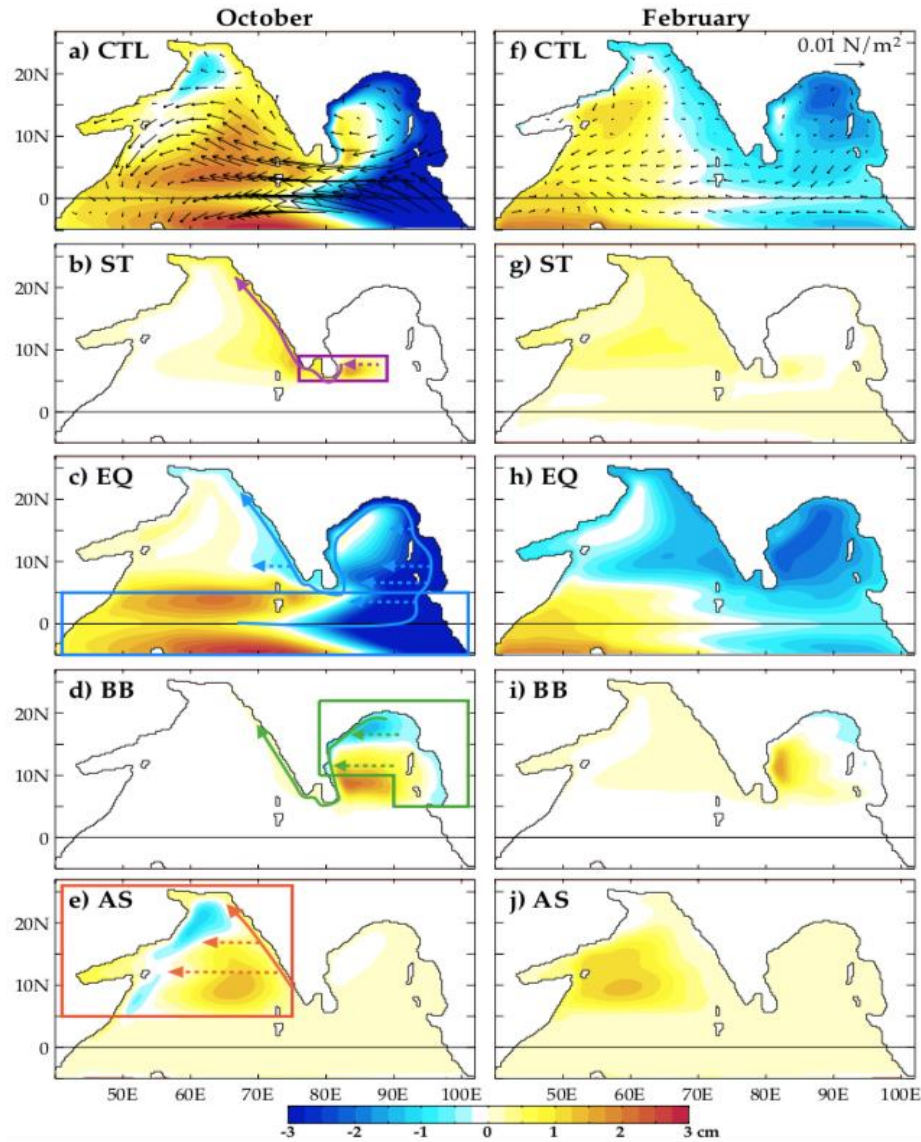


Figure 2. Typical IOD basin-scale SLAs and contributions from forcing in various regions, obtained as lead/lag regressions of the (a-e) October and (f-j) February interannual anomalies onto normalizedSON-averaged DMI for (a,f) CTL SLA and windstresses and decomposition of CTL SLA into (b,g) STIP forcing or ST process (purple box and arrows); (c,h) equatorial forcing or EQ process (light blue); (d, i) BoB forcing or BB process (green); and (e,j) Arabian Sea forcing or AS process (red). The ST, EQ, BB and AS contributions add up to CTL, owing to model linearity. Arrows symbolize the pathways of equatorial and coastal Kelvin waves (continuous) and Rossby waves (dashed).

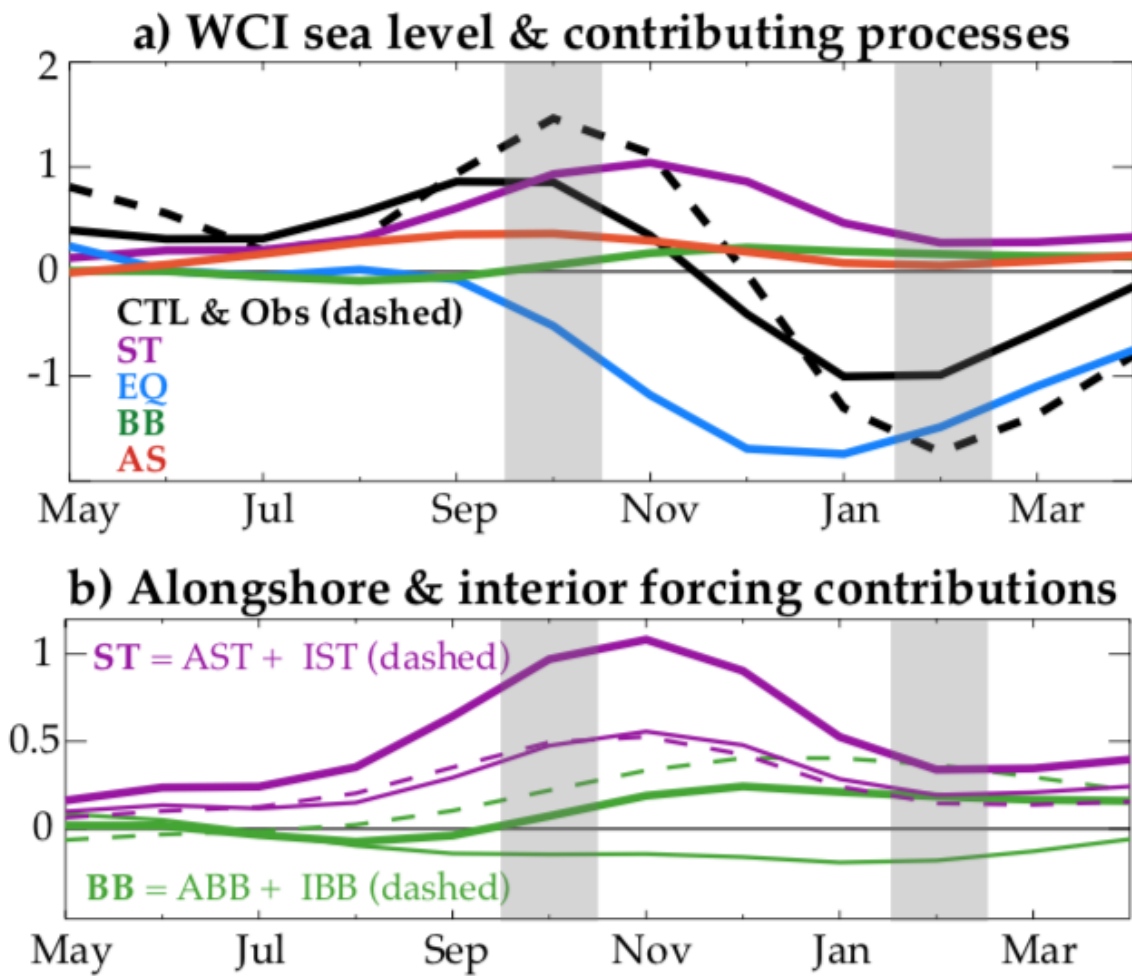


Figure 3. Typical IOD SLA along WCI and contributing processes, obtained as lead/lag regressions of interannual SLA (*cm*) on WCI box (Fig. 1a) to normalizedSON-averaged DMI for (a) CTL (continuous black), with its observed counterpart (dashed black), and its decomposition into ST (purple), EQ (light blue), BB (green), and AS (red) processes. (b) BB and AS processes (thick continuous) are further decomposed into alongshore (thin continuous) and interior wind-stress curl (thin dashed) forcing contributions. The grey vertical strips mark October and February, for which basin-scale patterns are displayed on Figure 2.

Supporting Information for

Sea level interannual variability along the west coast of India

I. Suresh¹, J. Vialard², M. Lengaigne^{2,3}, T. Izumo^{2,3}, V. Parvathi¹, and P.M. Muraleedharan¹

¹ CSIR-National Institute of Oceanography (CSIR-NIO), Goa, India

² LOCEAN-IPSL, Sorbonne Université (UPMC, Univ Paris 06)-CNRS-IRD-MNHN, Paris, France

³ Indo-French Cell for Water Sciences, IISc-NIO-IITM-IRD Joint International Laboratory, CSIR-NIO, Goa, India

Contents of this file

1. Details of the linear, continuously stratified ocean model
2. Details of the sensitivity experiments
3. Figures in support of the main text
 - a. Figure S1 shows the amplitude of seasonal and interannual sea level variability in the Indian Ocean
 - b. Figure S2 shows that the interannual sea level variability 1st Empirical Orthogonal Function (EOF1) is dominated by the influence of the Indian Ocean Dipole (IOD)
 - c. Figure S3 complements the main text Figure 2 by showing the patterns of sea level anomalies and wind-stress forcing associated with an IOD event for August, October, December, and February.
 - d. Figure S4 provides theoretical travel times of first baroclinic mode Rossby waves in the Bay of Bengal (BoB)
 - e. Figure S5 provides the process decomposition of west coast of India (WCI) signals separately for positive and negative IODs, allowing to discuss their asymmetrical influence on the WCI
 - f. Figure S6 completes the main text Figure 3 by showing typical IOD signals (and their process decomposition) in other relevant regions

1. The linear, continuously-stratified ocean model

We use the same linear, continuously stratified (LCS) model as that used to study the West Coast of India (WCI) intraseasonal variability and seasonal cycle in Suresh et al. (2013; 2016). This model is a modified version of the one presented in McCreary et al. (1996). The equations of motion are linearized about a state of rest with a realistic background stratification derived from the averaged Indian Ocean (15°S-15°N, 40°E-100°E) World Ocean Atlas (Locarnini et al., 2010) climatological potential density profile, and the ocean bottom is assumed flat. With these conditions, the solutions are represented as a sum of vertical normal modes, which are eigenfunctions, $\psi_n(z)$, satisfying the equation, $\left(\frac{1}{N_b^2} \psi_{nz}\right)_z = -\frac{1}{c_n^2} \psi_n(z)$, subject to the boundary conditions, $\psi_{nz}(-D) = \psi_{nz}(0) = 0$, where $N_b(z)$ is the Brunt–Väisälä frequency and $D (= 4000 \text{ m})$ is the ocean depth. The eigenvalue, c_n , of the above equation represents the characteristic Kelvin wave speed of the n -th mode. We use the first 5 baroclinic modes, the characteristic speeds of which are 252 cm s^{-1} , 155 cm s^{-1} , 88 cm s^{-1} , 69 cm s^{-1} , and 53 cm s^{-1} , but a very similar solution is obtained when using 20 modes instead, as in Suresh et al. (2013; 2016).

The response of each mode is obtained on a regular, 0.25° -resolution grid over a domain that covers the Indian Ocean from 30°S to 30°N and from 30°E to 110°E , and with a coastline determined by the 200-m isobaths (Smith & Sandwell, 1997), a good proxy for the continental shelf break. Vertical mixing has the same form as McCreary et al. (1996), but with a 7-year dissipation time scale for the first baroclinic mode. The horizontal mixing coefficient is set to $5000 \text{ m}^2 \cdot \text{s}^{-1}$. Wind is introduced into the ocean as a body force with the same profile (constant down to 50 m and ramped to zero at 100 m) as in McCreary et al. (1996).

The model is forced with daily TropFlux wind-stress anomalies (long-term mean removed) during 1979-2013 (available from <http://www.incois.gov.in/tropflux/>) (Praveen Kumar et al., 2013). We refer to this solution as the control (CTL) experiment.

2. Details of sensitivity experiments

The processes that influence the sea level along the WCI are discussed in detail in the main text (refer to Section 3.2). The contribution of each process is isolated using set of experiments with dampers and/or special boundary condition applied in specific regions.

The dampers are constructed as in McCreary et al. (1996) from a Newtonian damping which allows the waves to decay over a region of interest with an e-folding scale of $1.5 \Delta x$, where Δx is the grid size. To avoid distortions in the solutions, the Newtonian damping coefficients are ramped

linearly to zero within 1° from the edges of the damping region. As demonstrated in Suresh et al. (2016), our results are not very sensitive to the specific choice of these dampers or ramp. The solution obtained with such a damper will thus be free from the effect of waves emanating from this region. The dampers in our experiments are designed such that their edges match and the ramping coefficients add up to 1 there. That is, the sum of the various process solutions is exactly equal to the CTL experiment, owing to the linearity of the model.

As in McCreary et al. (1996), we also use the following special boundary condition in some sensitivity experiments:

$$\begin{aligned}\bar{\mathbf{u}}_n &= \mathbf{n} \cdot \mathbf{v}_n = -\mathbf{n} \cdot \left(\mathbf{k} \times \frac{\mathbf{F}_n}{f} \right) \\ \bar{v}_n &= (\mathbf{k} \times \mathbf{n}) \cdot \mathbf{v}_n = 0,\end{aligned}$$

where \mathbf{n} is a unit vector perpendicular to the coast, \mathbf{k} is an upward-directed unit vector, and f is the Coriolis parameter. $\mathbf{v}_n = (u_n, v_n)$ with \bar{u}_n, \bar{v}_n the horizontal components of velocity perpendicular and parallel to the coast. $\mathbf{F}_n = (F_n, G_n)$ where F_n and G_n are given by $F_n = \tau^x Z_n / (\bar{\rho} H_n)$ and $G_n = \tau^y Z_n / (\bar{\rho} H_n)$. τ^x and τ^y are the zonal and meridional wind stresses, and $H_n = \int_{-D}^0 \psi_n^2 dz$ and $Z_n = \int_{-D}^0 Z(z) \psi_n(z) dz$ are the coupling factors. The vertical profile, $Z(z)$, used here follows that of McCreary et al. (1996), which is constant down to 50 m and ramped to zero at 100 m. The second equation in the above represents no slip condition. The effect this boundary condition is to filter out alongshore forcing of coastal Kelvin waves, by allowing the Ekman flow to pass through the boundaries and hence generating no convergence and sea level anomaly at the coast.

In this paper, we carry out a series of sensitivity experiments to separate out the processes mentioned in Section 3.2. These experiments are essentially the same ones presented in Suresh et al. (2016).

The equatorial forcing process (EQ) is isolated using a damper over the entire equatorial region between 4°S and 4°N (light blue box on Fig. 2c in the main text; experiment EXP1), with a 1° ramp at the northern and southern edges to minimize distortion of the signal near the edges. The solution obtained with this damper has no signals emanating from the equatorial region, *i.e.* no equatorial forcing. CTL-EXP1 thus yields northern Indian Ocean sea-level variations resulting from equatorial forcing.

The BoB forcing process (BB) is isolated in an experiment with both the equatorial and BoB dampers (light blue and green boxes on Fig. 2cd; EXP2). EXP2 will thus be free from both EQ and

BB signals. EXP1-EXP2 hence yields the BB contribution to sea-level variability. We further isolate the contribution of the BoB alongshore forcing (ABB) by applying the special boundary condition described above within the BoB (green box on Fig. 2d; EXP2'). CTL-EXP2' hence isolates the effect of ABB forcing. The BoB interior Ekman pumping contribution (IBB) is further obtained by subtracting ABB from BB solution.

The ST process, which includes the alongshore forcing (AST) near the southern tip of India and Sri Lanka and the Ekman pumping due to wind-stress curl off the east coast of Sri Lanka (IST), is separated out by using an additional damper near the southern tip of India, extending up to 90°E (purple box on Fig. 2b; EXP3; i.e. EXP3 has dampers in the EQ, BB & ST regions). The difference EXP2-EXP3 thus yields the effect of ST (both alongshore forcing and Ekman pumping east of Sri Lanka). We further isolate the contribution of AST in the ST process in an experiment EXP3' in which we impose the special boundary condition described above within the purple box. CTL-EXP3' hence isolates the effect of alongshore forcing. The IST contribution is further obtained by subtracting this AST contribution from the ST process.

The effect of local alongshore forcing along the WCI is finally obtained by applying the special boundary condition along the entire WCI, in addition to all the above dampers (EXP4). EXP3-EXP4 thus isolates the effect of WCI winds. At the same time, EXP4 does not have the effect of equatorial, BoB and southern tip of India forcing and is also free from the effect of WCI alongshore winds. It has only the effect of interior wind forcing in the Arabian Sea. Both the above processes constitute the AS process.

The linearity of our model ensures that $EQ+BB+ST+AS=CTL$, except for numerical errors, which are orders of magnitude smaller than any of the components. As noted above, the BB, ST and AS contributions can further be decomposed into interior (I) and alongshore (A) contributions, e.g. $ST=IST+AST$.

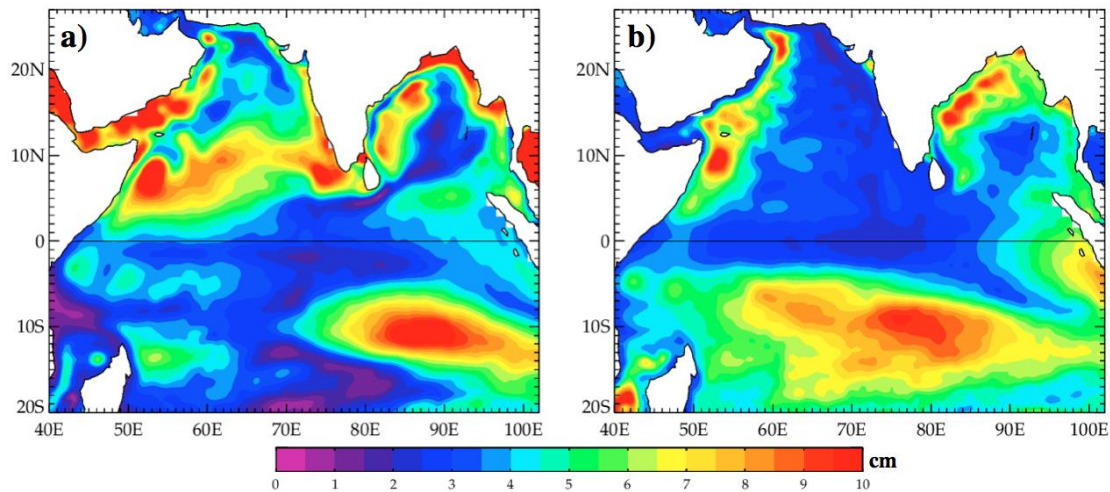


Figure S1: Standard deviation of the observed sea level a) seasonal cycle and b) interannual anomalies.

Take-home message(s): The amplitude of sea level seasonal cycle is much larger than the interannual variability along the WCI. The sea level interannual variability is much larger in the BoB than along the WCI. This probably explains why previous studies discussed the seasonal cycle on the WCI (e.g. Suresh et al. 2016; because of its high amplitude) or the interannual variability in the Bay of Bengal (e.g. Aparna et al. 2012; because it has a high amplitude) but not the interannual variability on the WCI (because of its relatively weaker amplitude). While the WCI SLA interannual variability is weak, it has strong societal impacts. Parvathi et al. (2017) indeed showed that even small perturbations in the WCI thermocline/oxycline depths during SON can potentially trigger/suppress anoxic conditions, due to the upwelling-driven shallow thermocline/oxycline depths at this time of the year. Those anoxic conditions have strong societal impacts, owing to their adverse influence on ecosystems and fisheries. This emphasizes the need for better understanding of the WCI interannual sea level variability (see introduction section in the text for more details)

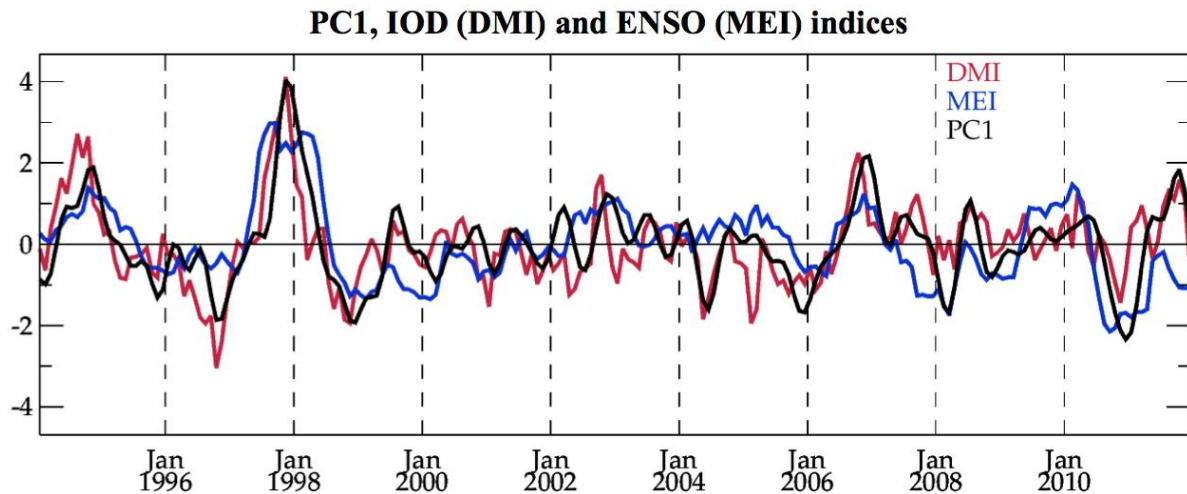


Figure S2: Normalized first principal component (PC1, black) of the northern Indian Ocean interannual monthly sea-level anomalies from the CTL experiment, along with the normalized Dipole Mode index (DMI, red) and multivariate ENSO Index (MEI, blue).

Take-home message(s): PC1 has a higher correlation with DMI Index during the IOD peak (SON; 0.95) than with MEI index during ENSO peak (NDJ; 0.81). In line with the previous literature on the subject (see the main text), this indicates that the EOF1 captures the intrinsic sea-level variability associated with the IOD, rather than that associated with the ENSO.

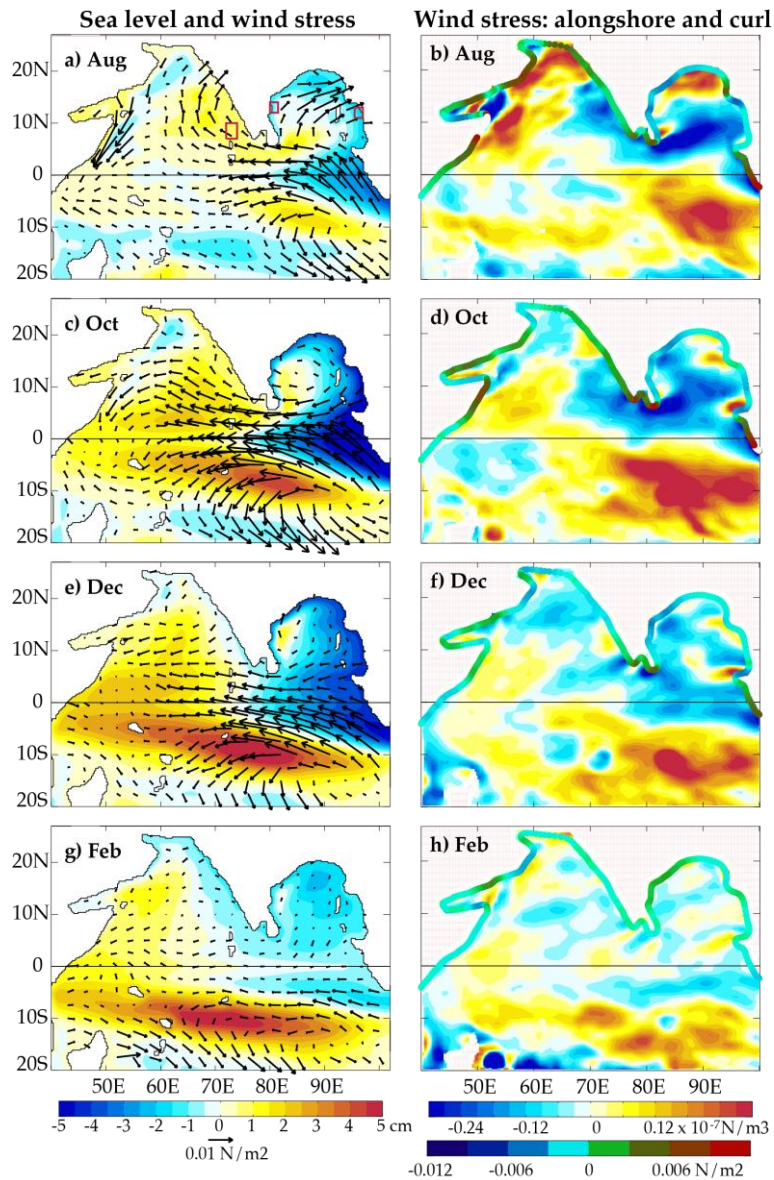


Figure S3: Maps of (left column) CTL SLA (cm) and wind-stress ($N.m^{-2}$) vectors and (right column) wind-stress curl ($N.m^{-3}$; shading) and alongshore wind stresses ($N.m^{-2}$; shading along the coastline) lead-lag regression onto the normalized SON-averaged DMI during (a, b) August; (c, d) October; (e, f) December; and (g, h) February. Red boxes marked on panel a will be used in Figure S5.

Take-home message(s): Typical sequence of wind forcing and sea-level response associated with a positive IOD event. Note that the west coast of India signals shift from positive in boreal fall to negative in winter.

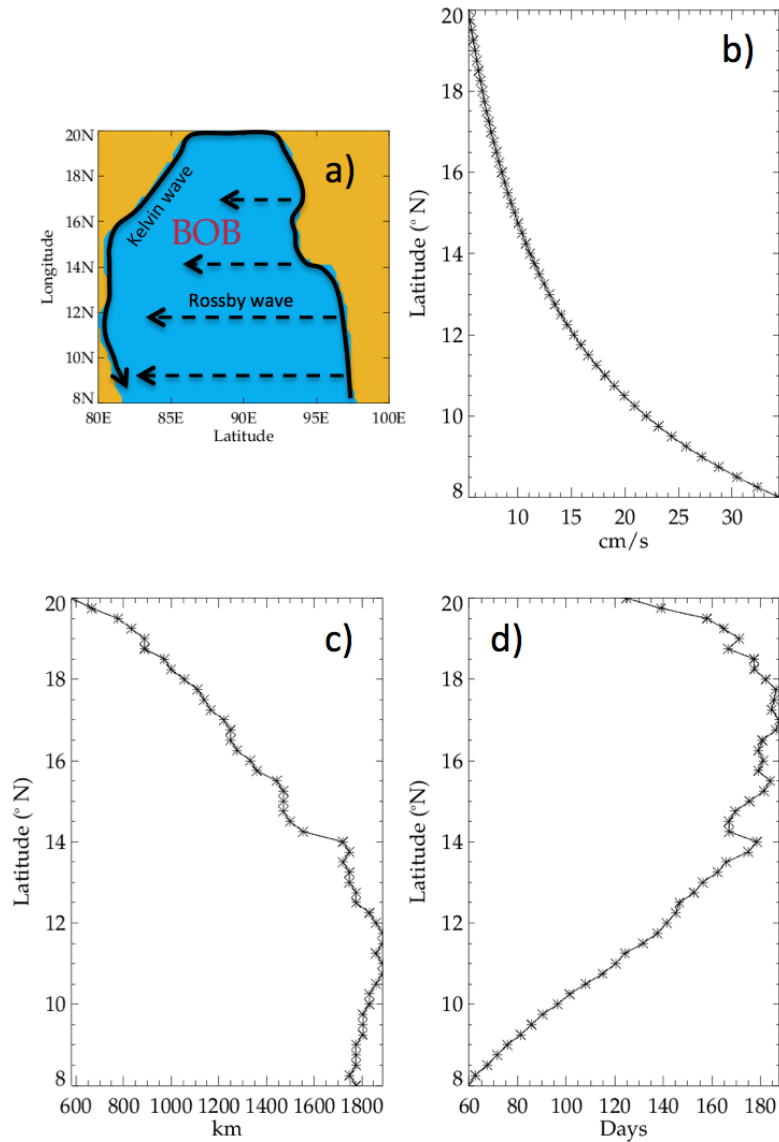


Figure S4: a) Sketch showing the pathways of coastal Kelvin and mid-latitude Rossby waves travelling from one given latitude on the eastern rim to the same latitude on the western rim of the BoB. Also shown, as a function of latitude, are b) Rossby wave phase speed, computed with a typical first baroclinic wave speed of 2.5 m.s^{-1} , c) distance across BoB basin, d) Rossby wave travel time to cross the basin.

Take-home message(s): A first-baroclinic mode coastal Kelvin wave typically takes ~ 20 days (with 2.5 m.s^{-1}) to travel around the BoB coastal waveguide ($\sim 4300 \text{ km}$), while Rossby waves typically need 2 to 6 months, depending on the latitude, to cross the BoB basin.

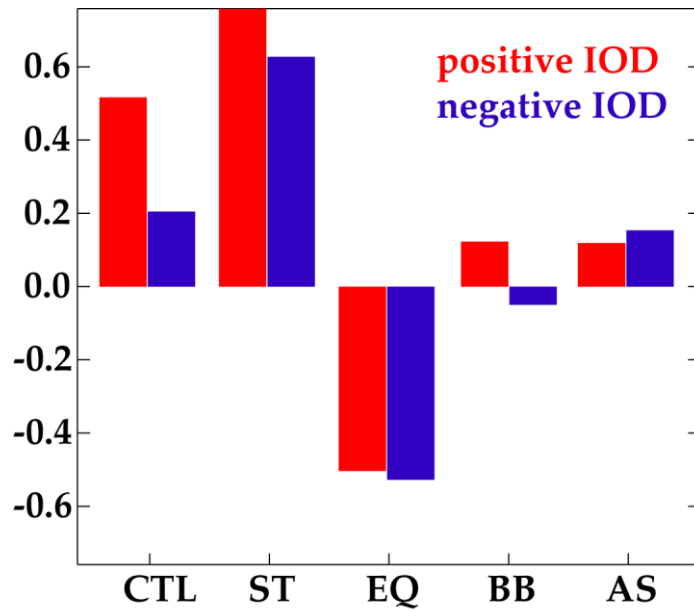


Figure S5: Regression of WCI CTL interannual sea-level anomalies in SON to the normalized SON-averaged DMI during a typical positive (red; i.e. regression only for $DMI > 0$) and negative (blue; i.e. regression only for $DMI < 0$) IOD events, and its decomposition into the ST, EQ, BB, and AS processes.

Take-home message(s): For a given IOD amplitude, the WCI sea-level response is larger for positive IODs, due to stronger ST and BB processes, which can be linked to zonal equatorial wind anomalies that extend more northward during positive IOD than their negative counterpart.

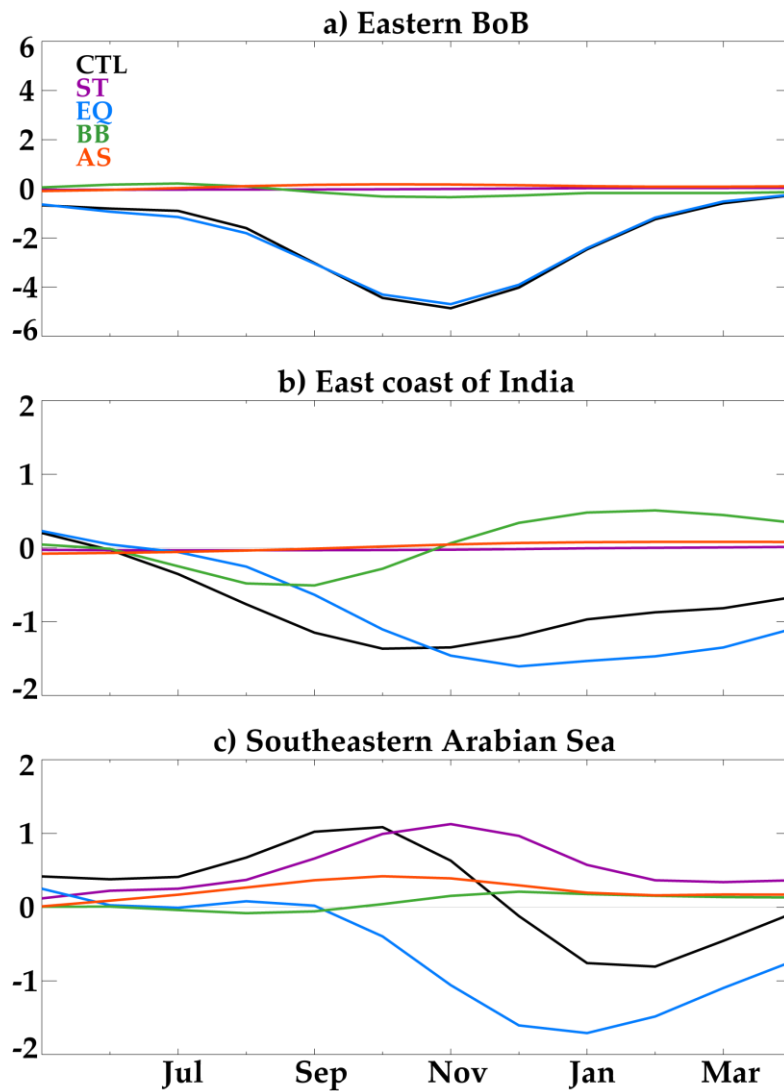


Figure S6: Same as Figure 3 in the main text, but for coastal locations on the a) eastern BoB; b) east coast of India; c) southeastern Arabian Sea, indicated by red frames in Figure S3a.

Take-home message(s): Sea-level signals are almost entirely associated with equatorial remote forcing in the eastern BoB. Local BoB forcing starts contributing (but rather weakly) along the east coast of India, where EQ is still the most dominant process. The contributing processes to the sea level interannual variability in the southeastern Arabian Sea are very similar to those along the WCI (Fig. 3 in the main text), i.e., the ST and EQ, but with a slightly stronger contribution of Arabian Sea local forcing.